Selective catalytic reduction of NO by NH3 on cerium modified faujasite zeolite prepared from aluminum scraps and industrial metasilicate

Rahma Abid, Gérard Delahay, Hassib Tounsi

Selective catalytic reduction of NO by NH_3 on cerium modified faujasite zeolite prepared from aluminum scraps and industrial metasilicate

RahmaAbid[1], Gérard Delahay[2], HassibTounsi[1]

[1]Laboratoire des matériaux avancés, Ecole Nationale d'Ingénieurs de Sfax, Université de Sfax, TUNISIE.

[2]Institut Charles Gerhardt, CNRS/UM/ENSCM, Equipe "Matériaux Avancés pour la Catalyse et la Santé", Ecole Nationale Supérieure de Chimie de Montpellier, 240 av. du Professeur Emile Jeanbrau, 34296 Montpellier cedex, France

Abstract

This work was devoted to the study of the selective catalytic reduction of NO by NH_3 on calcined and hydrothermal treated cerium loaded zeolite catalysts. The parent faujasite zeolite Na-F (Si/Al = 1.32 and S_{BET} = 749 m^2/g) used as support for the preparation of the catalysts was obtained from industrial sodium metasilicate and aluminum scraps. As expected, the NO conversion increased with increasing the percentage of cerium in the structure of the faujasite zeolite. Total NO conversion into N_2 was reached at 400°C at a space velocity of 250,000 h^{-1}. The high conversion is due to the redox shift between Ce^{3+}/ Ce^{4+} and the strong acid sites related to the rare earth present in the framework that is the key in SCR of NO process. Moreover, the highest loaded cerium catalyst retained high almost its activity after thermal hydrotreatment at 850°C. This higher loading is desirable for both activity and stability provided that two stages of preparation are used to put the Ce ions in the sodalite cages.

Keywords: Aluminum Scraps, Ce-Y, NH_3-SCR, Hydrothermal stability.

1. Introduction

The nitrogen oxide NO is a harmful gas which is produced during combustion of fossil fuels at high temperatures. It is essentially issued from mobile or stationary sources by oxidation of the nitrogen of the air. The major sources that produce NO are the fossil fuels like coal in the electrical power plants or fuels in the engines of gasoline and diesel cars[1]. NO is harmful to health and environment; it contributes to death and serious respiratory illness like asthma,

chronic bronchitis [2], [3]. Furthermore, NO acidifies surface water (acid rain) reducing biodiversity and killing fishes. It is also damage forest ecosystem and contribute to the decreaseofvisibility by the formation of the ‘’smog’’. For these reasons, the emissions of NO must be limited.

The NO molecule is thermodynamically unstable. Nevertheless, it does not decompose because of its high activation energy (364kJ/mol). Thus, a catalyst must be used to facilitate its decomposition and reduced it to N_2 and water [4, 5]. The oxygen produced from the decomposition of NOor the gaseous mixture strongly adsorbed on the active sites of catalyst which causes their poisoning[5]. To avoid this inhibiting effect on the transformation rate of NO, it is necessary to work in the presence of reducing agents like H_2, NH_3, hydrocarbon (HC)[6, 7].The most common technology in the elimination of NO is the selective catalytic reduction of NO by NH_3 (NH_3-SCR). Two main types of catalysts are commercially used for this technology: V_2O_5-WO_3/TiO_2 and Cu,Fe-zeolites. For the former type of catalyst, vanadium, which is toxic sublimes at high at high temperature. Moreover, it shows high oxidation of SO_2 to SO_3 which leads to decrease the activity and selectivity of NO_x at 400°C[8–10]. For these reasons, copper and iron exchanged zeolites have been developed and are preferred for mobile Diesel sources [11–13]. In the last decades, the cerium-catalysts were investigated in the NH_3-SCR of NO because of its redox property (Ce^{3+} to Ce^{4+}) that promotes the activation of reactants on the surface of the catalysts[14, 15]. The redox shift between Ce^{4+} and Ce^{3+} of CeO_2 can promote NO oxidation to NO_2, which is beneficial to the NH_3-SCR reaction[16]. As such, CeO_2 has been widely used as key component of selective catalytic reduction catalyst for NO_x removal such as CeO_2/TiO_2[17], CeO_2/Al_2O_3[18], CeO_2/zeolite[19], Mn-Ce/TiO_2[20]. It had been reported that ceria based catalyst has great resistance to SO_2 and H_2O poisoning in the NH_3-SCR reaction[21]. Wang et al. [22]investigated the influence of cerium precursor in the NH_3-SCR of NO at low

temperature. They found that the catalyst prepared from $Ce(NO_3)_3.6H_2O$ precursor (Ce−NO-R) with nanorods morphology exhibits higher NO_x conversion and superior SO_2/H_2O resistance. Zhang et al. [23] studied the ceria loaded zirconium phosphate catalysts in NH_3-SCR. They found that the addition of 20 wt.% ceria to zirconium phosphate catalyst exhibited more than 98% NO_x conversion and 98% N_2 selectivity in a wide temperature window of 250–425 °C[23]. Carja et al. [24] studied the reduction of NO by NH_3 on Mn-Ce/ZMS-5 catalysts which present NO conversion about 75-100% in the temperature range of 244-550 °C. The work reported by Qi et al. [25] demonstrated a good NO conversion at 120°C of MnOx-CeO_2 catalyst. Wu et al. [26] showed that the introduction of cerium on MnO_x/TiO_2catalyst leads to steady NO conversion of 84 % in the presence of SO_2 for 6.5hours in the reaction stream. Compared to MnO_x/TiO_2 catalyst, there is a largely decrease of NO conversion to 30 %.

In this work, the reduction of NO by NH_3 on fresh and hydro-treated cerium-Faujasite zeolite catalysts was investigated. The parent zeolite Na-F (Si/Al = 1.32 and S_{BET} = 749 m^2/g) used as support for the preparation of catalysts was obtained from industrial sodium metasilicate and aluminum scraps. Moreover a large part of this study was devoted to the characterization of fresh and hydro-treated cerium-Faujasite zeolite catalysts by different techniques (XRD, FTIR, BET, UV–vis and H_2-TPR)

2. Experimental

2.1 Materials

Industrial sodium metasilicate ($Na_2SiO_3.5H_2O$, PQ CORPORATION) was used as silicon source for the preparation of the FAU zeolite. The aluminum source‘s was aluminum scraps collected from metal manufacturing industry in the region of Sfax(Al= 99.77% ± 0.02, Fe= 0.207± 0.006 and Cu= 0.008±0.001).The other chemical products are sodium hydroxide

pellets (NaOH, Sigma Aldrich 99% purity) and cerium (III) chloride heptahydrate $CeCl_3.7H_2O$ (Sigma Aldrich 99, 99%).

2.2 Preparation of the zeolitc support

Firstly, NaOH pellets were dissolved in the required quantity of distilled water. Then the alkaline solution was divided to equal volumes in polypropylene bottles. The desired quantity of aluminum scraps was dissolved in one half of hydroxide solution volume and then filtered to remove the impurities. The silicon sources was added to the other half of hydroxide solution volume and mixed in capped bottle until clear. In order to obtain the aluminosilicate hydrogel, the silicon solution was poured to the aluminum solution quickly. The obtained thickly gel was stirred during a period of 10 min and then was aged for 14 h at room temperature (RT). Finally, the aged gel was heated at 80°C for 6 and 24hours. After the crystallization was achieved, the obtained solids were filtered, washed with distilled water until pH around 9, and then dried at 80°C for 24h.

2.3. Preparation of the catalysts

Cerium-zeolite faujasite (Ce-F) catalysts were prepared by ionic exchange method in aqueous solution by varying the concentration of cerium chloride: 0.02 M; 0.01 M and 0.005M. The required amount of cerium chloride was dissolved in 50mL of distilled water and then 1g of Na-F zeolite were added to the solution and mixed for 5 h at 50 °C. The slurry was then centrifugated, washed three times with distilled water to remove the non-exchanged cerium and adsorbed chlorides on the surface of the zeolite. The recovered solids were dried for 24h at 80 °C and then calcined for 1 hour at 450 °C. The obtained catalysts were called Ce(x)-F, with x the cerium amount in wt%.

Another catalyst called Ce(20)-F_C was also prepared using 0.02M of cerium chloride solution. Nevertheless, after drying at 80 °C, the powder was calcined for 1 hour at 750 °C to

ensure the siting of cerium in the sodalite cages. Finally, it was exchanged another time with 0.02M of cerium chloride solution and then calcined for 1 hour at 450 °C.

2.4 Characterization and analysis

The obtained samples were characterized by a variety of conventional techniques. Powder X-ray diffraction (XRD) patterns were obtained using D8 ADVANCE BRUKER 40 Kv with Cu Kα radiation. The diffraction pattern was collected in the 2θ range of 5-50° at a scan speed of 0.02°. The prepared zeolite was compared with a commercial Na-Y zeolite (Aldrich, cat. no 33,444-8, lot 06402LR, Si/Al=2.5). Infrared spectra were scanned from 400 to 4000 cm^{-1} using the FourierTransform infrared model Perkin Elmer spectrum BX spectrometer. The scanning electron microscopy (SEM) images were taken on a Hitachi S 4800 operated at 5Kv. The BET surface areas (S_{BET}) and pore size distributions were determined by nitrogen adsorption–desorption on an ASAP2020 instrument (Micromeritics Instrument Corporation, GA. Prior to these measurements, the samples were degassed at 250 ◦C in vacuum.Thermogravimetric analysis (TGA) experiments were carried out on Perkin Elmer Simultaneous Thermal Analyser STA 6000 under anair at a flow rate of 100 cm^3 min^{-1}. The temperature increased from 30 to 900 °C at a rate of 10 °C/min. H_2-TPR studies were conducted on a MicromeriticsAutochem 2910 instrument. 80 mg of oven dried sample was placed in one arm of a U-shaped quartz tube on quartz wool. Prior to TPR, the catalysts samples were pretreated with 20% O_2/N_2 at 550 ◦C for 30 min (10°/min) to remove the water present, then are cooled in air at 50 ° C. The TPR analysis was carried out in a reducing mixture consisting of 3% H_2/Ar and heated from 50 to 800°C (10 °C/min). UV/Vis diffuse reflectance spectra were collected by Lambda 40 Perkin spectrometer.

The NH_3-SCR of NO catalytic test was performed in temperature programmed surface reaction (TPSR, 5°C/min)) using a flow reactor operating at atmospheric pressure with a

space velocity of 250,000 h^{-1}. The catalyst sample (24 mg) was putted in quartz reactor positioned between two layers of inert quartz wool. The reactant gas composition was adjusted to 1000ppm NO, 1000ppm NH_3, 8 % O_2, 3.5 % H_2O and balance with helium.

Hydrothermal treatment of catalysts was carried out in quartz fixed-bed microreactor. However, 1 g of catalyst was placed in the reactor and heated to the desired temperature in flowing 20% O_2/He. Then water is injected by circulating the airflow through a bubbler containing deionized water at 47 °C (10% H_2O vapour) during 4 hours. All gas lines were heated to prevent water condensation. Four different hydrothermal temperatures were used: 700°C (ht 700), 800°C (ht 800), 850°C (ht 850) and 900°C (ht 900). The resulting solids were labeled Cu(x)-F ht XXX).

3. Results and discussions

3.1. Characterization of the prepared zeolitesErreur ! Nous n'avons pas trouvé la source du renvoi.

The molar composition of the starting gel used to study the effect of crystallization time is the following: **5.19 Na_2O: Al_2O_3:2.9 SiO_2:182.76 H_2O**. After aging for 14 hours at room temperature, the gel was crystallized at 80°C for 6 and 24 hours.

Figure 1 shows the XRD patterns of the obtained solids at 80°C for 6h(Na-F_{6h}) and 24h(Na-F_{24h}). After 6 h of crystallization, one can see fine diffraction peaks characteristic of the FAU zeolite. The increase of the crystallization time to 24 h, there is an increase of the intensity of the peaks.

In table 2, we reported the chemical analysis of the two samples Na-F_{6h} and 24 h Na-F_{24h} performed by EDS in five different spots. The Si/Al molar ratios of the two samples are comparable; Si/Al= 1.27 for Na-F_{6h} and Si/Al = 1.32 for 24 h Na-F_{24h}[27].

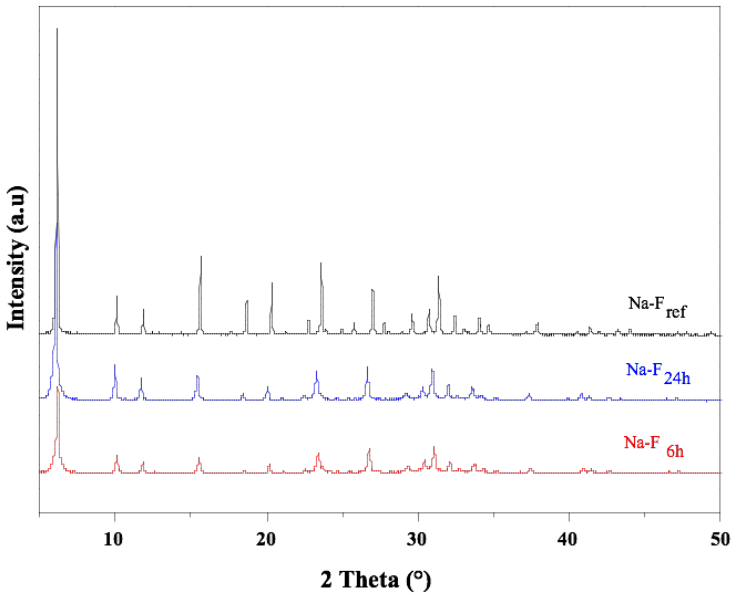

Figure 1 : XRD of Na-F_{6h}, Na-F_{24h} prepared at 80°Cfor 6 and 24 hours, respectively.

Table1 : Chemical analysis of Na-$F_{6h,}$ Na-F_{24h}samples performed with EDS.

Samples	Na (wt. %)	Al (wt.%)	Si (wt. %)	Si/Al (mol/mol)
Na-F_{6h}	19.62	35.26	46.74	1.27
Na-F_{24h}	21.07	33.95	46.97	1.32

The SEM micrographs of Na-F24h (A1, A2) were displayed in **Figure 2**. The micrographs showed some crystals fused together forming agglomerate particles. Moreover, the particle size of isolated crystals was less 1µm. It can be seen from the image that the catalyst shows perfect degree of crystallization which is in accordance with the XRD results (

Figure 1). In the rest of the work we use the sample Na-F_{24h} and it will be named Na-F.

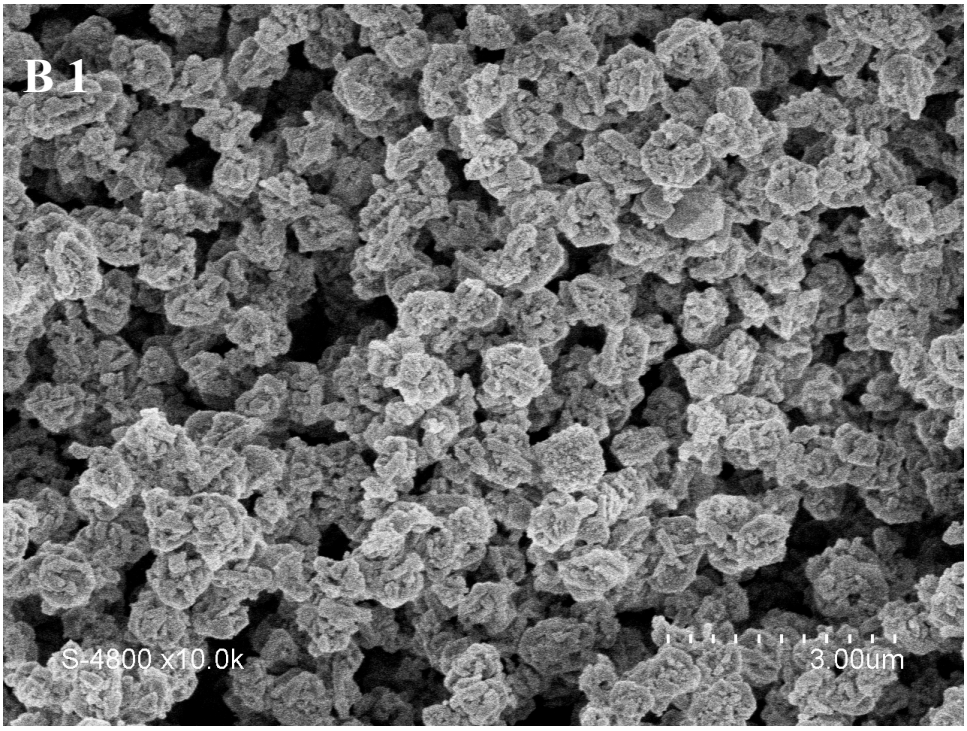
B 1
S-4800 x10.0k
3.00um

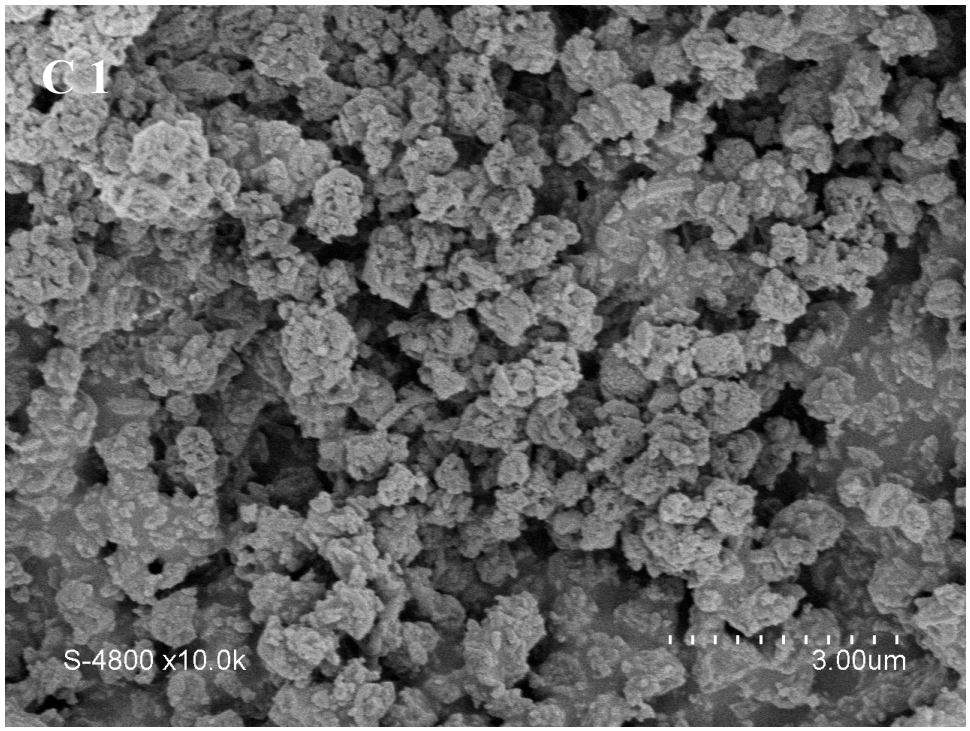
C 1
S-4800 x10.0k
3.00um

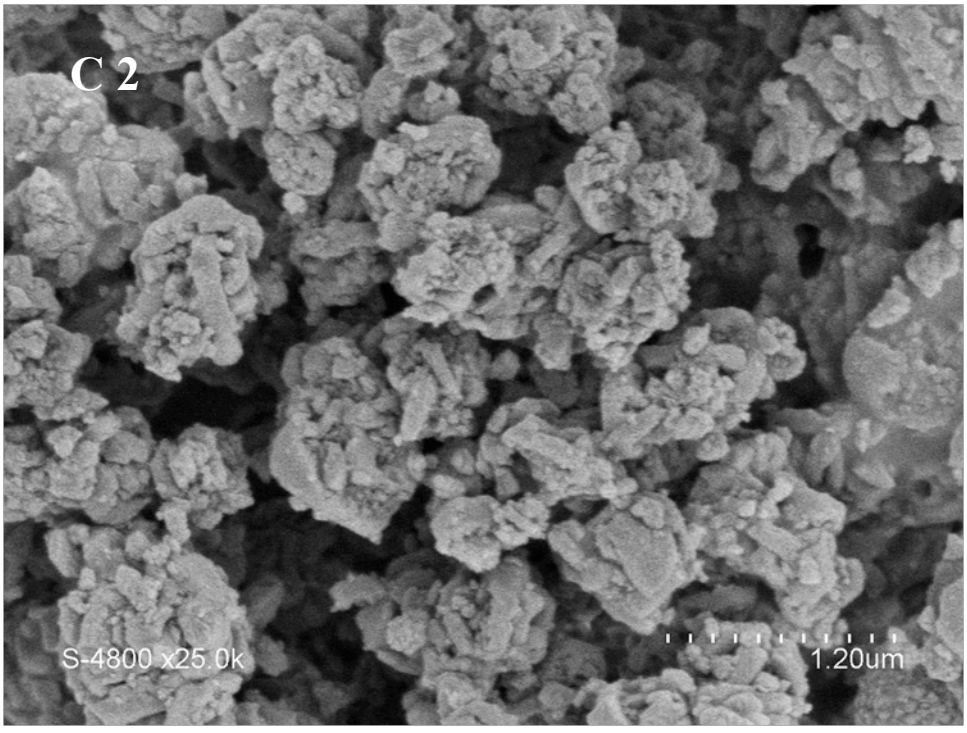
C 2
S-4800 x25.0k
1.20um

Figure 2 : SEM of (A1, A2) Na-F, (B1, B2) Ce (5)-F, and (C1, C2) Ce (20)-F_c.

The FTIR spectrum of **Na-F zeolite** was reported in **Erreur ! Nous n'avons pas trouvé la source du renvoi.** We found at 560 cm^{-1} the characteristic band related to the double six ring (D6R) in the faujasite zeolites[28]. The bands at 666 $cm^{-1}$and 957cm^{-1} can be attributed to TO_4 symmetric and asymmetric stretching vibration modes of Si-O, respectively. The peak at 447 cm^{-1} was attributed to T-O bending mode. The peak at 745 cm^{-1} is characteristic for symmetric stretching vibrations of external linkages[29]. The peak at 1646 cm^{-1} can be assigned to the bending mode of physically adsorbed water. According to Flanigen et al.[30], the T-O band near 455 cm^{-1} for the zeolite FAU type Y contains a high-frequency shoulder which is not present in zeolite FAU type X. Also, the 406 cm^{-1} pore opening band present in X zeolite is not found in Y zeolite.

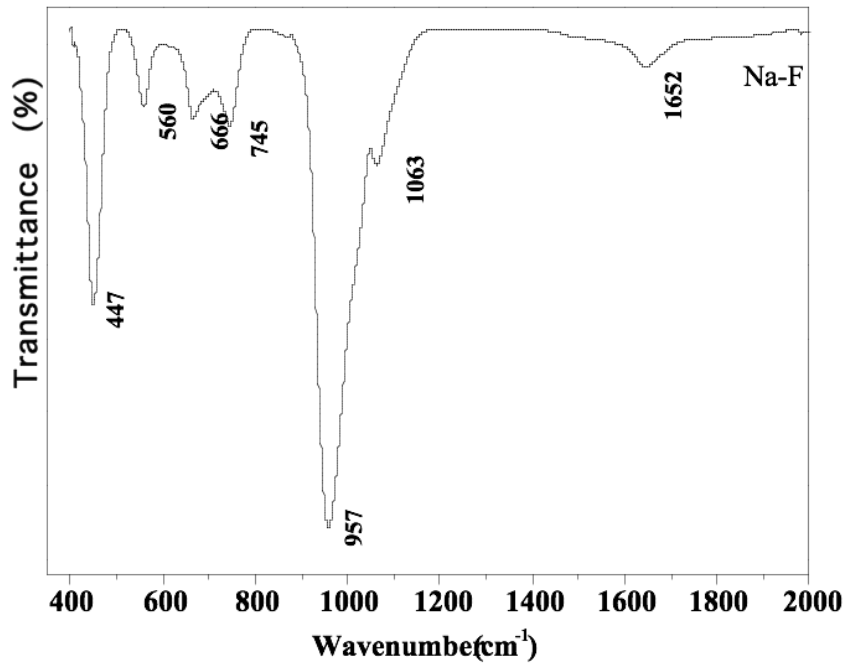

Figure 3 : FTIR spectrum of Na-F zeolite.

3.2.Characterisationof the prepared catalysts

Figure 4 showed the XRD patterns of the carrier Na-F and the Ce-exchanged catalysts Ce(5)-F, Ce(10)-F, Ce(20)-F and Ce(20)-$F_{C.}$ The XRD catalyst profiles demonstrate only peaks relative to the zeolite FAU without any supplementary peaks of cerium oxide or other Ce based phases. Thus, one can conclude that the cerium cations are not agglomerated and well dispersed into the zeolite porosity [30, 31]. In general, with calcination at high temperature (>300 °C), cerium ions located in the supercages starts to migrate to the sodalite cage and are stabilized by the framework oxygens [33]. All catalysts have a light yellow color, this observation indicates the presence of cerium tetravalent[34].

On the other hand, the crystallinity of the catalysts decreased as the percentage of cerium increased. This feature can be explained by the removal of Al atoms from the framework without the destruction of the structure [32] due to the siting of cerium in the sodalite cages. It indicated that cerium had a strong interaction with the matrix of the zeolite[35].

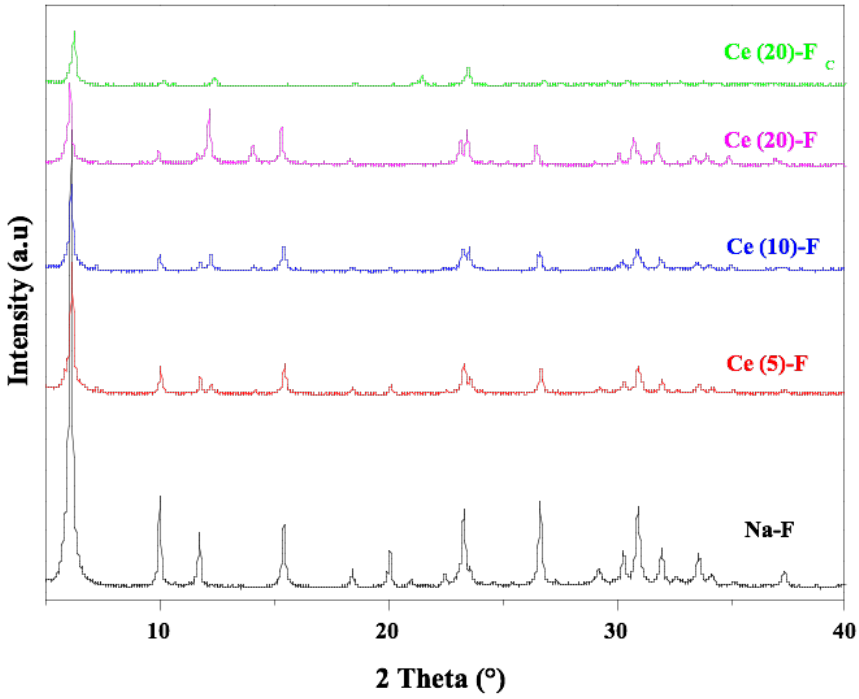

Figure 4 : XRD of Na-F, Ce (5)-F, Ce (10)-F, Ce (20)-F and Ce (20)-F_C

The SEM micrographs of catalysts Ce (5)-F (B1, B2) and Ce (20)-F_C (C1, C2) are reported in**Figure 2**. From this analysis we demonstrate that the two catalysts have the same morphology of the zeolite Na-F (**Figure 2**) with nanoscale crystals. Nevertheless, it was observed an agglomeration which is due to the interconnection of small particles, but the cerium particles is not observed in this magnification because they presented in a small amount.

Erreur ! Nous n'avons pas trouvé la source du renvoi. presents the nitrogen adsorption-desorption isotherms of the samples Na-F, Ce (5)-F, Ce (10)-F, Ce (20)-F and Ce (20)-F_C. A typical type I adsorption isotherm is obtained in each case, indicating that the solids are microporous according to the classification ofIUPAC[36]. The presence of hysteresis loop from 0.66 to 0.98 arises indicated the presence of mesoporous from the packing of zeolite nanocrystals[37]. In Erreur ! Nous n'avons pas trouvé la source du renvoi. were reported the BET surface area S_{BET} external surface, micropore volume and micropore surface area of the samples Na-

F, Ce (5)-F, Ce (10)-F, Ce (20)-F and Ce (20)-F_C. The BET total surface area (S_{BET}) has changed under the condition of different Ce percentages from low to high with respect to microporous materials of Na-F zeolite itself, which possess rich specific surface area (S_{BET}= 749m^2/g). The introduction of the rare earth cations causes a decrease in the micropore surface area and volume. It is attributed to the existence of the cerium cations or extra-framework aluminum species in the cages or channels blocking the pore structure[38].

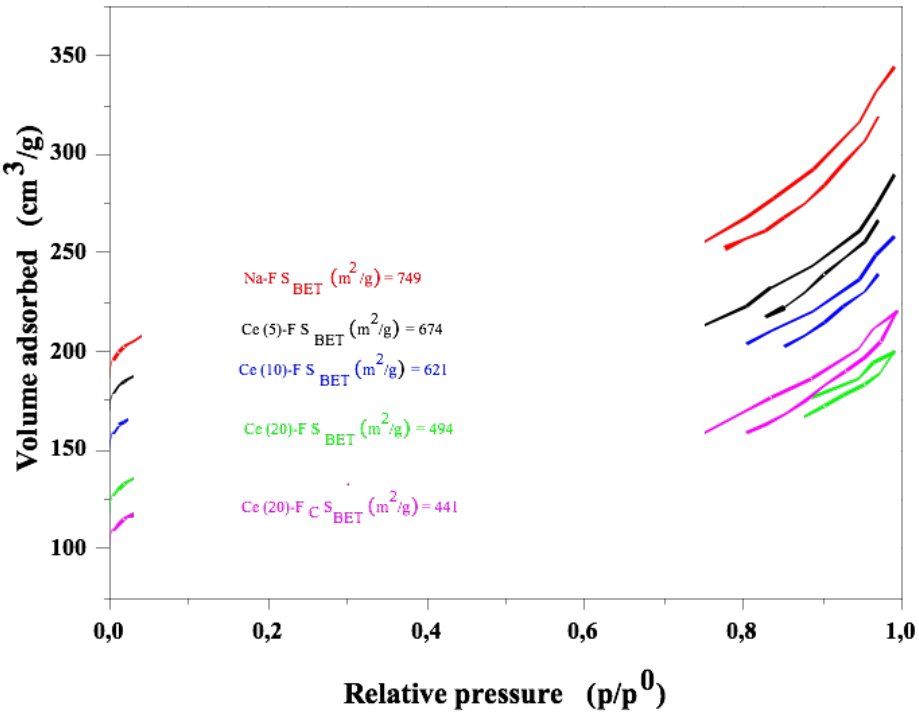

Figure 5 : BET of Na-F, Ce (5)-F, Ce (10)-F, Ce(20)-F and Ce(20)-F_C.

Table 2 : BET surface area, external surface, micropore volume and micropore surface area of the samples Na-F, Ce (5)-F, Ce (10)-F, Ce (20)-F and Ce (20)-F_C.

Catalyts	S_{BET} (m^2/g)	$S_{external}$(m^2/g)	$V_{micropore}$(cm^3/g)	Micropore area (m^2/g)
Na-F	749	121	0.28	628

Ce(5)-F	674	81	0.27	592
Ce(10)-F	621	82	0.24	538
Ce(20)-F	494	75	0.19	418
Ce(20)-F_C	441	105	0.15	335

The TGA/DTGA profiles of three samples were displayed in

Figure 6. The Na-F, Ce(20)-F and Ce(20)-F_C show a mass loss at the range of temperature (30-400°C) corresponding to water adsorbed on the surface and that present in the zeolite channels contributing to 21%, 25%, and 18% of their total masses, respectively.

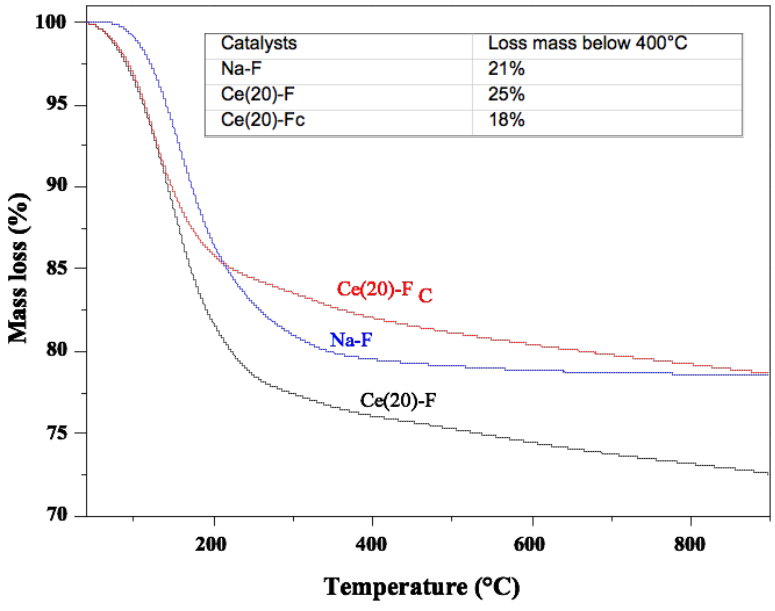

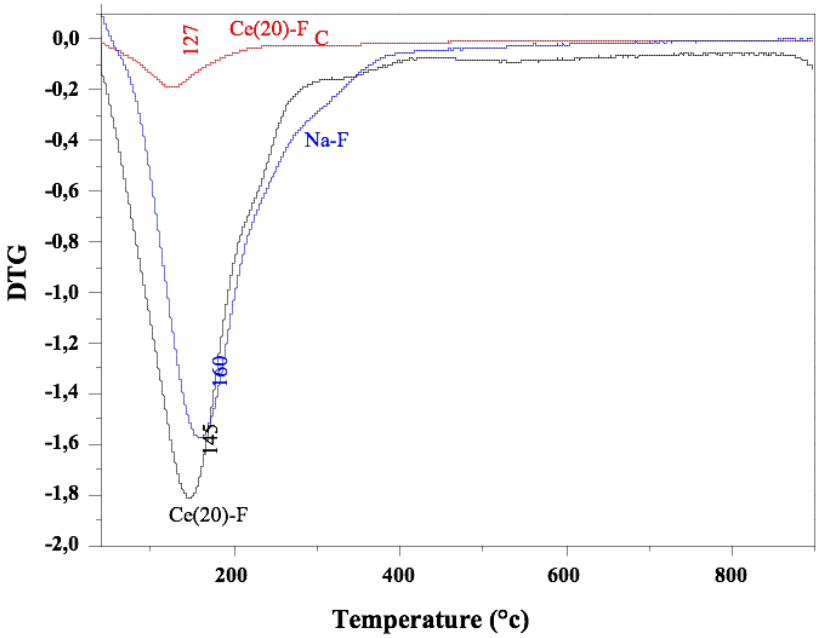

Figure 6 : TGA/DTGA of Na-F, Ce(20)-F and Ce(20)-F_C.

The diffuse reflectance UV-Vis spectroscopy is used to identify and characterize the metal ion coordination and its existence in metal position in the framework and/or extra-framework of zeolite. The diffuse reflectance UV-Vis spectra of catalysts Ce (5)-F, Ce (10)-F, Ce (20)-F, Ce (20)-F_C and $CeO_2$are reported in

Figure 7.It showed single peak at ~ 310 nm and its intensity increases with an increase in the Ce content of the samples. This band may be attributed to the charge transfer from O 2p to Ce 4f. The electronic transitions from oxygen to cerium need more energy for a hexa-coordinated than tetra-coordinated Ce^{4+}. So, the band at 310 nm is due to the presence of one type of well-dispersed Ce^{4+} species probably in a tetra-coordinated environment[39]. For the pure ceria, the profile showed two peaks at 256 and 347nm. According to the literature [40] pure ceria presents three peaks at 255, 285 and 340nm. The first peak corresponds to O^{2-} to Ce^{3+}

charge transfer. Whereas, the other two peaks may be attributed to the O^{2-} to Ce^{4+} charge transfer (285nm) and interband (340nm) transition.

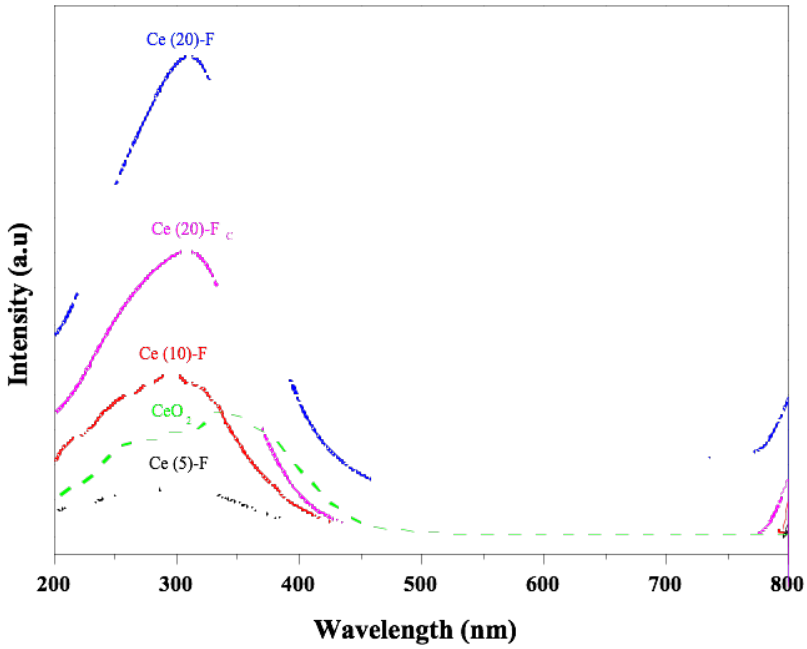

Figure 7 : UV-vis spectroscopy of Ce (5)-F, Ce (10)-F, Ce (20)-F, Ce (20)-F_C and CeO_2**.**

The H_2-TPR analysis was used to study the reducibility of Ce present in the catalysts. The reduction profiles of the different catalysts (Ce (5)-F, Ce (10)-F and Ce (20)-F_C) and CeO_2 (Sigma Aldrich 316970) are reported in

Figure 8. The profile of the pure CeO_2 presents two reduction peaks. The first one at lower temperature (520°C) can be related to the reduction of the surface capping oxygen Ce^{4+}-O-Ce^{4+}. The second peak at high temperature around 890°C correspond to the reduction of oxygen in the bulk (elimination of O^{2-})[41]. For the three catalysts Ce(5)-F, Ce(10)-F and Ce(20)-F_C, the large peaks around 527, 557 and 512°C, respectively were attributed to the

reduction of Ce^{4+} to Ce^{3+}. It is noted that the H_2 consumption increases with the increasing of the quantity of cerium in zeolite. For the catalyst Ce(20)-F_C, the deconvolution of the reduction profile showed two peaks at 461 and 541°C. The first one could be attributed to the reduction of Ce^{4+} ions present in the supercages whereas the second one to the reduction of Ce^{4+} ions in the sodalites ~~presence of larger cerium aggregates on the external surface of the zeolite and the second one can be related to isolated cerium species~~[42]. With the two steps preparation including the high temperature of calcinations, Ce ions may enter are in the S_I sites coordinated with three oxygen atoms of the zeolitic framework and have substituted the sodium in the sodalite cages. Ce^{4+} ions located in the sodalites are more difficult to be reduced. ~~For that reason, the H_2 consumption is refer to the oxide existing in the surface and in the supereage of zeolite [43]~~.

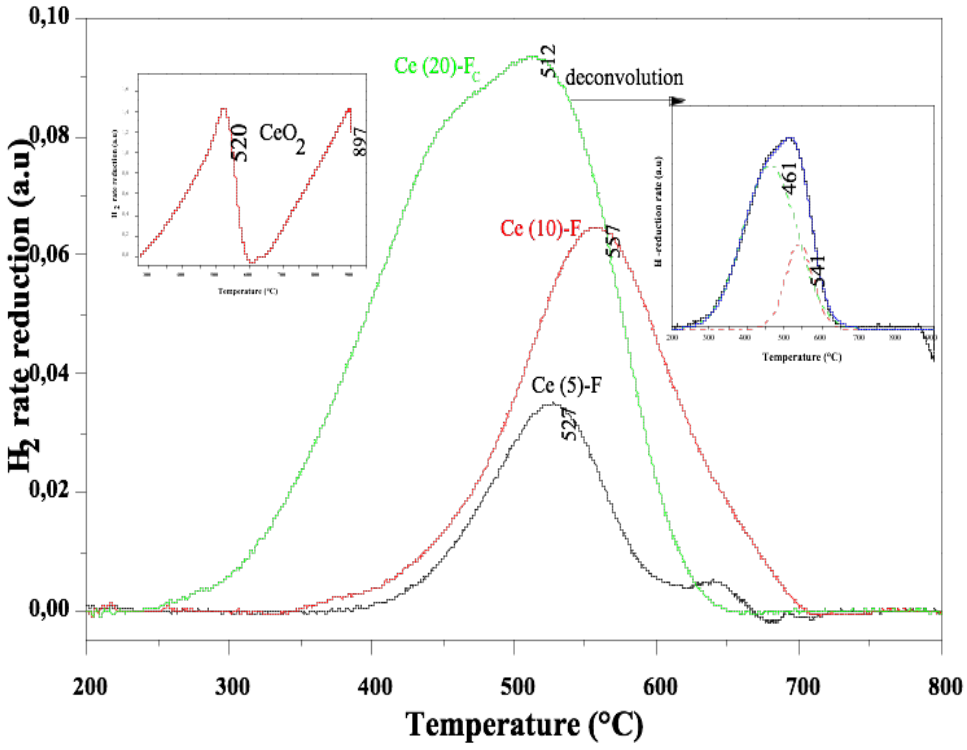

Figure 8 : H_2-TPR of Ce (5)-F, Ce (10)-F and Ce (20)-F_C and pure CeO_2.

3.3Selective catalytic reduction of NO by NH_3

3.3.1 NO conversion of fresh catalysts

The NO conversion to N_2 of Fresh catalysts Ce (5)-F, Ce (10)-F, Ce (20)-F, Ce (20)-F_C and Na-F are shown in

Figure 9. At first, it should be mentioned that catalysts do not produce N_2O over the whole range of studied temperatures. The support Na-F presents a poor NO conversion about 12% at 550 °C. The introduction of cerium to Na-F zeolite produces marked changes in the catalytic behavior. As seen for the less exchanged catalyst Ce(5)-F, the NO conversion increased from 2% at 250°C to 55% at 500°C. The further increase of cerium content in the catalysts; Ce(10)-F and Ce (20)-F enhanced the NO conversion. The catalyst Ce(10)-F showed an increase of NO conversion from 6% at 250 to 88% at 500°C and then remained constant (88% of NO conversion) above this temperature. For the catalyst Ce(20)-F, NO conversion is already of 40% at 200°C and then, it increased gradually with the increase of temperature and reached 100% of NO conversion at 400°C. Compared to Ce(20)-F catalyst, Ce (20)-F_C was less active at temperatures below 400 °C but NO conversion reached 100% at 500 °C.On the other hand, the light-off temperature (T50), the maximum NO conversions and the related temperatures of Ce(5)-F, Ce(10)-F and catalysts were reported in Table 3. It can be seen that Ce(20)-F catalyst is more active and has the lowest light-off temperature than the other catalysts.

Furthermore, with the increase of cerium content for Ce(x)-F catalysts there was a decrease of the T50 and an increase of the NO conversions.

As said before, withthe increase of cerium content there was an increase of NO conversion in the whole temperature range. Literature reported that the high activity cerium catalysts in theNH_3-SCR[44] is due to the redox property of Ce^{4+}/Ce^{3+} couple. Indeed, in the presence of oxygen, Ce^{3+}oxidized toCe^{4+} which oxidizesNO to NO_2, in low temperature region, which is among the key steps in theNH_3-SCR. The cerium have a redox property like the others transition metal, but the cerium have orbital f which make the distribution of catalytic sites, like oxygen vacancies, especially in the case of surface redox reactions[44], e.g. bonding with molecules like nitric oxides[45].Also the orbital 4f of Ce^{4+}cation, in the surface, has the capacity to store and release reversibly or selectively electrons, so this property can have an impact in the stabilization of adsorbed reactants and induced their reactions. So the presence of sufficient oxygen vacancies on the surface is the key to initiate the co-adsorption of NO and the later reaction for the formation of N_2 [44].

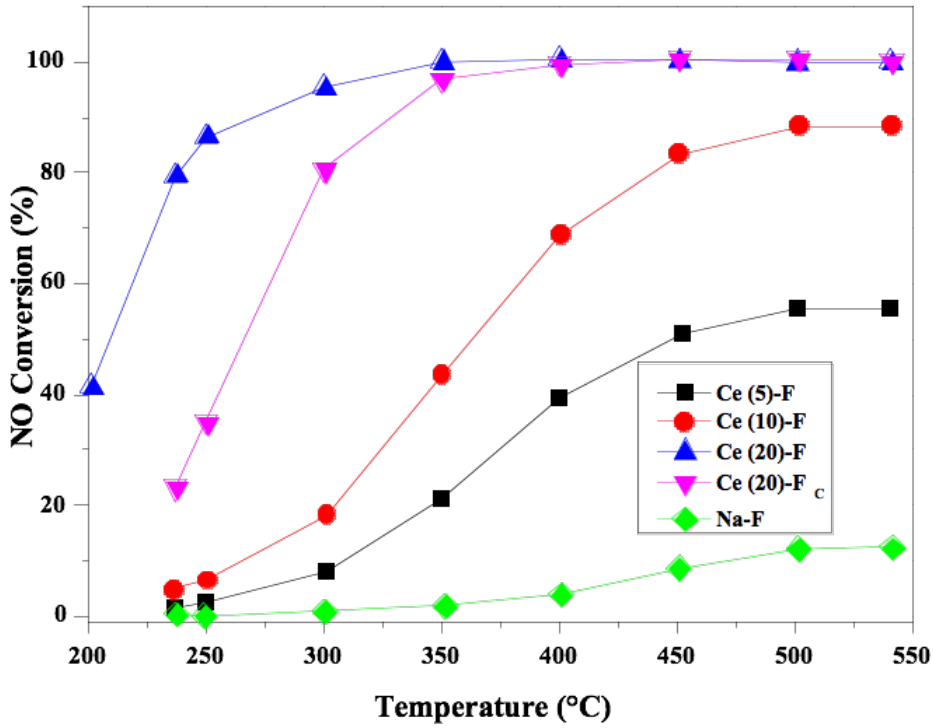

Figure 9 : The NO conversion of Fresh catalysts Ce (5)-F, Ce (10)-F,Ce (20)-F, Ce (20)-$F_C$and Na-F support.

Table 3: The light of temperatures, the maximum NO conversions and the related temperatures of prepared catalysts.

Catalysts	T_{50} (°C)	NO Con (%)	T max (°C)
Ce(5)-F	452	55	500
Ce(10)-F	365	88	500
Ce(20)-F	210	100	350
Ce(20-F_C	267	100	400

3.3.2 Hydrothermal stability

An hydrothermal treatment at high temperature is usually used for simulating the ageing of the NH_3-SCR catalysts for the automotive applications. To study the effect of hydrothermal treatment, two sets of experiments were performed by aging all catalysts at 700 and 800°C for 4 hours in the presence of 10% of water vapor.**Figures 10and 11** reported the NO conversions of the hydrotreated catalysts Ce(x)-F at 700 and 800°C for 4 hours in the presence of 10% of water vapor, respectively. After hydrothermal treatment at 700 ˚C (

Figure 10 : **Hydrothermal treatment of Ce(5)-F, Ce(10)-F, Ce(20)-F and Ce(20)-FC at 700°C for 4hours.**

), all aged catalysts show different degrees of activity loss at high temperatures compared with fresh catalysts. However, for the catalyst with highest cerium content Ce(20)-F_C ht700 shows a slight degradation of NO conversion throughout the temperature range. . In table 4, we reported the NO conversions of fresh and aged catalysts at 500°C. From these results, it is noted that when the percentage of cerium increases the catalyst remains stable after hydrothermal treatment and has a good NO conversion. Indeed, the Ce(20)-Fht700 catalyst presents 96 % of NO conversion at 500 °C compared to Ce(5)-Fht700 which presents only 22 %. On the other hand, for the

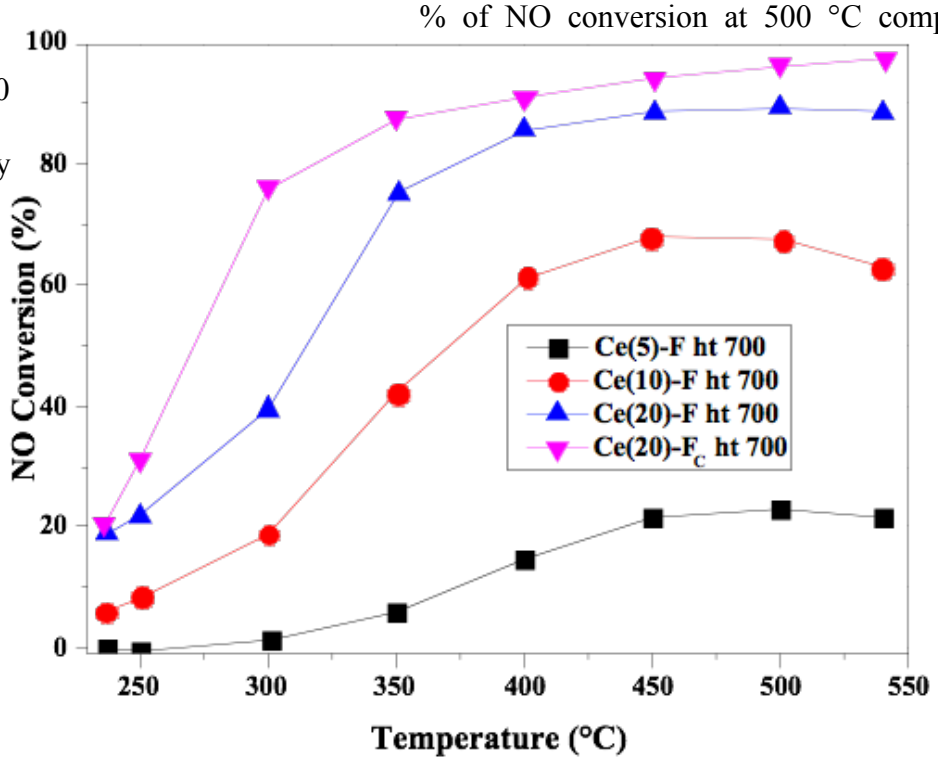

hydrotreated catalysts at 800°C, one can observe that the increase of the aging temperature has a remarkable influence on the catalytic performance. For the two catalysts Ce(5)-Fht800 and Ce(10)-Fht800,NO conversions drastically decreased to16 % and 13%, respectively. Furthermore, the catalyst Ce(20)-Fht800 presents only 81% of conversion at 500°C. But for the Ce(20)-F_C ht800 the conversion remains stable (96% of NO conversion) at 500°C. The above results indicate that Ce(20)-F_C ht800 is more stable than other catalysts during the hydrothermal treatment. Because of its hydrothermal stability the catalyst Ce(20)-F_C ht800 was tested after undergoing higher hydrothermal treatment temperature, 850 and 900 ° C, for 4 hours.

Figure 10 : Hydrothermal treatment of Ce(5)-F, Ce(10)-F, Ce(20)-F and Ce(20)-F_C at 700°C for 4hours.

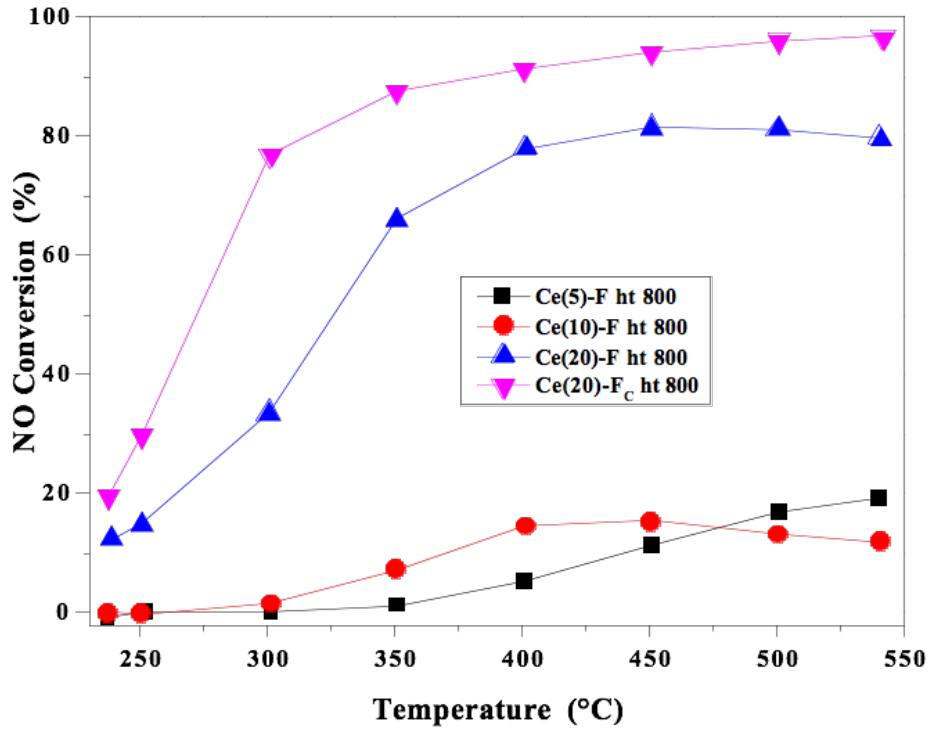

Figure 11 : Hydrothermal treatment of Ce(5)-F, Ce(10)-F, Ce(20)-F and Ce(20)-F_C at 800°C for 4hours.

Table 4 : NO conversionsat 500°C of fresh and aged catalysts at 700 °C and 800 °C.

Catalysts	**NO Conv. Fresh catalysts (%)**	**NO Conv after H.T 700°C (%)**	**NO Conv.After H.T 800°C (%)**
Ce(5)-F	55	22	16
Ce(10)-F	88	67	13
Ce(20)-F	100	89	81
Ce(20)-F_C	100	96	96

Figure 12 presents the NO conversion of Ce (20)-F_C catalyst before and after hydrothermal treatment for 4 hours at 700, 800, 850 and 900°C. It is noted that the NO conversions decreased slightly from 100% for the fresh catalyst to about 95% for the catalysts: Ce (20)-$F_C$ht700, Ce (20)-$F_C$ht 800 and Ce (20)-$F_C$ht850. Nevertheless, after hydrothermal treatment at 900°C (Ce(20)-$F_C$ht 900) the catalytic activity was decreased to 12%. This reduction in the conversion is due to the destruction of the catalyst structure and the formation of cerium oxide at 28° and 47 ° as shown by the XRD (

Figure **13**).

The slight decrease of NO conversions for the catalysts hydrotreated at 700 °C, 800 °C and 850 °C can be related to the presence of cerium cations into the sodalite cages of the zeolite Na-F. Actually, during the preparation of the catalyst Ce (20)-F_C, the latter was calcined at higher temperature (750 °C) compared to the other catalysts (450 °C). The use of this higher calcination temperature permits to the cerium cations to migrate from the supercage to the sodalite cage and to form bridges with the oxygen framework which stabilize the zeolites tructure[46, 47]. Y. Shu et al. [46] reported that the hydrothermal treatment of zeolite catalysts at high temperatures (500-800°C), provokes the dealumination of the framework especially for those having low Si/Al ratio. So, the aluminum atoms migrate from their

positions and settle down in zeolite channels and cages. To moderate the deactivation of the zeolite catalysts rare earth cations like cerium was added to the formulation. The addition of cerium prevented the framework dealumination, and preserved the acid sites, which greatly ameliorated the hydrothermal stability.

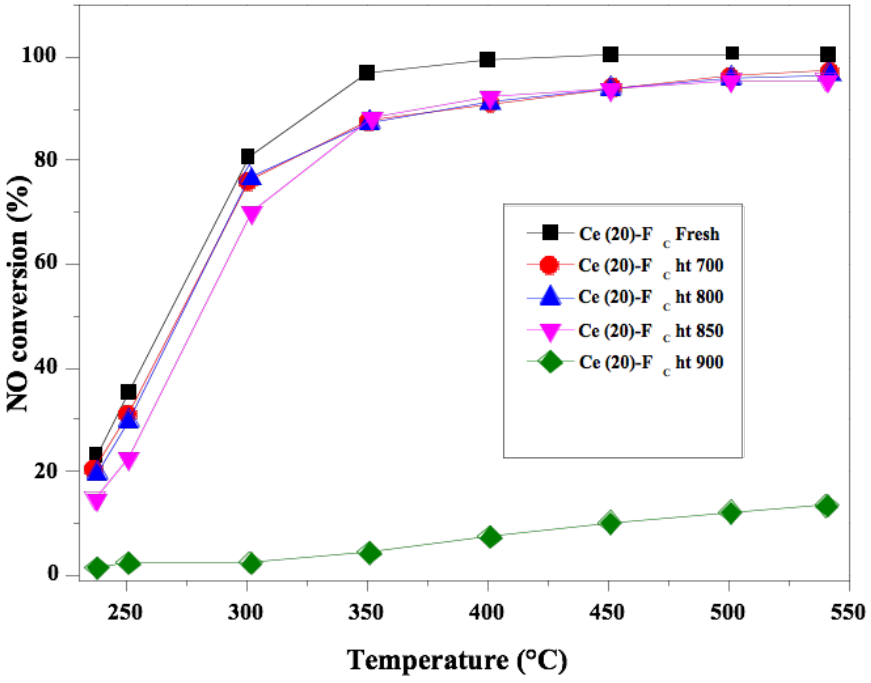

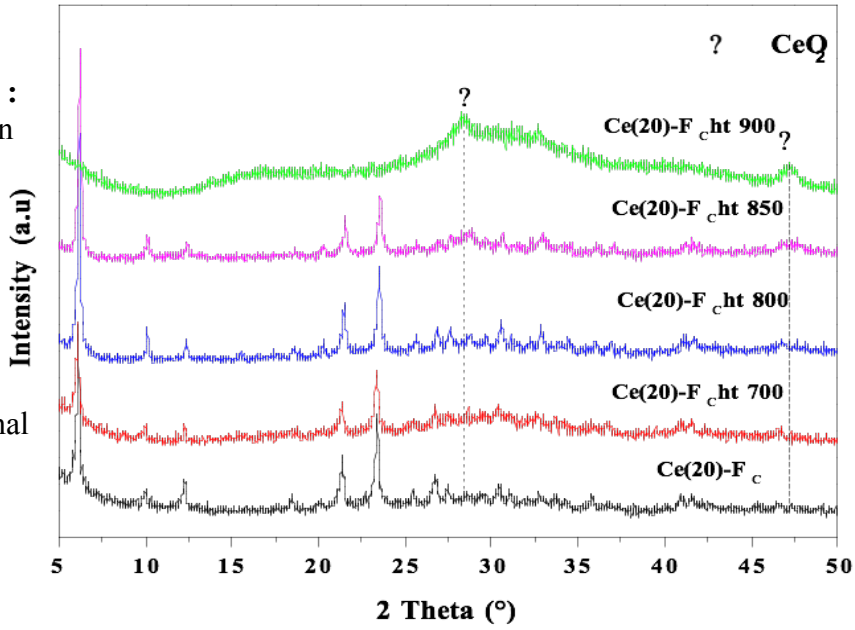

Figure 12 : The NO conversion of catalysts Ce (20)-F_C before and after hydrothermal treatment 4h

at 700, 800, 850 and 900°C.

Figure 13 : XRD of catalyst Ce (20)-F_C before and after hydrothermal treatment 4h at 700, 800, 850 and 900°C.

4. Conclusion

In this study, FAU zeolite has been prepared using cheap starting materials; aluminum scrap and industrial sodium metasilicate with hydrogel molar composition **5.19 Na_2O : Al_2O_3 :2.9 SiO_2 :182.76 H_2O**. The obtained zeolite after hydrothermal synthesis at 80 °C for 24 h, has been used as carrier to prepare cerium exchanged catalysts with different cerium content.The NO conversion increased with increasing the percentage of cerium in the framework of zeolite. The best catalytic activities is concerned to the catalysts Ce(20)-F and Ce(20)-F_C catalyst. It should be underlined that, after hydrothermal treatment of the catalysts, Ce(20)-F_C at 850°C for 4 hours, NO conversion remains stable whereas for Ce(20)-F prepared by a classic way, a noticeable loss of activity is already observed after hydrothermal treatment at 800°C. The two steps procedure, allowing the siting of Ce ions into the sodalite cages of the

faujasite greatly improves the hydrothermal stability of the catalysts. Contrarly to copper faujasite, Ce-FAU catalysts shows hydrothermal stability comparable to other small pore zeolithe structures. The increase of the hydrothermal treatment temperature to 900°C leads to a drastic decrease of NO conversion to 12%. This behavior can be related to the destruction of structure of zeolite and the appearance of CeO_2 peaks as shown by XRD technique and is generally observed for the other zeolite structures.

References

[1] S. Brandenberger, O. Kröcher, A. Tissler, and R. Althoff, *The state of the art in selective catalytic reduction of NOxby ammonia using metal-exchanged zeolite catalysts*, vol. 50, no. 4. 2008.

[2] U.S. EPA, "Overview of the human health and environmental effects of power generation: focus on sulfur dioxide, nitrogen oxides, and mercury," *Clear Ski. Initiat.*, 2002.

[3] F. Gao *et al.*, *A Review on Selective Catalytic Reduction of NOx by NH3 over Mn–*

Based Catalysts at Low Temperatures: Catalysts, Mechanisms, Kinetics and DFT Calculations, vol. 7, no. 7. 2017.

[4] D. E. L. Ille, R. E. Catalytique, S. Des, O. D. Azote, L. H. Ou, and L. E. Methane, "L'u s t l," 2004.

[5] S. Roy, M. S. Hegde, and G. Madras, "Catalysis for NOxabatement," *Appl. Energy*, vol. 86, no. 11, pp. 2283–2297, 2009.

[6] M. König, K. Eisinger, I. Hartmann, and M. Müller, "Combined removal of particulate matter and nitrogen oxides from the exhaust gas of small-scale biomass combustion," no. X, 2018.

[7] M. Moreno-González, A. E. Palomares, M. Chiesa, M. Boronat, E. Giamello, and T. Blasco, "Evidence of a Cu2+–Alkane Interaction in Cu-Zeolite Catalysts Crucial for the Selective Catalytic Reduction of NOx with Hydrocarbons," *ACS Catal.*, vol. 7, no. 5, pp. 3501–3509, May 2017.

[8] X. You, Z. Sheng, D. Yu, L. Yang, X. Xiao, and S. Wang, "Influence of Mn/Ce ratio on the physicochemical properties and catalytic performance of graphene supported MnOx-CeO2 oxides for NH3-SCR at low temperature," *Appl. Surf. Sci.*, vol. 423, pp. 845–854, 2017.

[9] X. Yao *et al.*, "Selective catalytic reduction of NOx by NH3 over CeO2 supported on TiO2: Comparison of anatase, brookite, and rutile," *Appl. Catal. B Environ.*, vol. 208, pp. 82–93, 2017.

[10] L. Li *et al.*, "Ultra-low loading of copper modified TiO2/CeO2 catalysts for low-temperature selective catalytic reduction of NO by NH3," *Appl. Catal. B Environ.*, vol. 207, pp. 366–375, 2017.

[11] J. Grzybek, B. Gil, W. J. Roth, M. Skoczek, A. Kowalczyk, and L. Chmielarz, "Characterization of Co and Fe-MCM-56 catalysts for NH3-SCR and N2O decomposition: An in situ FTIR study," *Spectrochim. Acta Part A Mol. Biomol. Spectrosc.*, vol. 196, pp. 281–288, 2018.

[12] M. P. Ruggeri, I. Nova, E. Tronconi, V. Schmeißer, and M. Weibel, "Modelling the Hydrothermal Ageing of a Fe-Zeo- lite Catalyst for Automotive NH 3 -SCR Applications," no. 0, pp. 1–14, 2018.

[13] H. Wang, R. Xu, Y. Jin, and R. Zhang, "Zeolite structure effects on Cu active center, SCR performance and stability of Cu-zeolite catalysts," *Catal. Today*, 2018.

[14] L. Zhao *et al.*, "Simultaneous removal of elemental mercury and NO in simulated flue gas over V2O5/ZrO2-CeO2 catalyst," *Appl. Catal. B Environ.*, vol. 198, pp. 420–430, 2016.

[15] X. Wang, Z. Chen, Y. Wang, and R. Wang, "Rare- Earth- Doped Pt/Ba/Ce0. 6Zr0. 4O2- Al2O3 for NOx Storage and Reduction: The Effect of Rare- Earth Doping on Efficiency and Stability," *ChemCatChem*, vol. 6, no. 1, pp. 237–244, 2014.

[16] R. Guo, Y. Zhou, W. Pan, J. Hong, and W. Zhen, "Journal of Industrial and Engineering Chemistry Effect of preparation methods on the performance of CeO 2 / Al 2 O 3 catalysts for selective catalytic reduction of NO with NH 3," *J. Ind. Eng.*

Chem., vol. 19, no. 6, pp. 2022–2025, 2013.

[17] X. Yao, L. Chen, J. Cao, F. Yang, W. Tan, and L. Dong, "Morphology and Crystal-Plane Effects of CeO2 on TiO2/CeO2 Catalysts during NH3-SCR Reaction," *Ind. Eng. Chem. Res.*, Aug. 2018.

[18] Q. Jin, Y. Shen, and S. Zhu, "Praseodymium Oxide Modified CeO 2 / Al 2 O 3 Catalyst for Selective Catalytic Reduction of NO by NH 3," pp. 1283–1290, 2016.

[19] A. K. Ingole, D. Dixit, and S. V Dingare, "A review on Selective Catalytic Reduction technique for diesel engine exhaust after treatment," vol. 7, no. 7, pp. 206–210, 2017.

[20] T. Boningari *et al.*, "Influence of elevated surface texture hydrated titania on Ce-doped Mn / TiO 2 catalysts for the low-temperature SCR of NO x under oxygen-rich conditions," *J. Catal.*, vol. 325, pp. 145–155, 2015.

[21] A. Manuscript, "Catalysis Science & Technology," 2015.

[22] X. Wang *et al.*, "E ff ect of Ceria Precursor on the Physicochemical and Catalytic Properties of Mn − W / CeO 2 Nanocatalysts for NH 3 SCR at Low Temperature," 2017.

[23] Q. Zhang *et al.*, "Applied Surface Science In situ DRIFTS investigation of NH 3 -SCR reaction over CeO 2 / zirconium phosphate catalyst," *Appl. Surf. Sci.*, vol. 435, pp. 1037–1045, 2018.

[24] G. Carja, Y. Kameshima, K. Okada, and C. D. Madhusoodana, "Mn–Ce/ZSM5 as a new superior catalyst for NO reduction with NH3," *Appl. Catal. B Environ.*, vol. 73, no. 1–2, pp. 60–64, 2007.

[25] G. Qi and R. T. Yang, "Performance and kinetics study for low-temperature SCR of NO with NH3 over MnOx–CeO2 catalyst," *J. Catal.*, vol. 217, no. 2, pp. 434–441, 2003.

[26] Z. Wu, R. Jin, H. Wang, and Y. Liu, "Effect of ceria doping on SO2 resistance of Mn/TiO2 for selective catalytic reduction of NO with NH3 at low temperature," *Catal. Commun.*, vol. 10, no. 6, pp. 935–939, 2009.

[27] M. M. J. Treacy and J. B. Higgins, *Collection of simulated XRD powder patterns for zeolites fifth (5th) revised edition*. Elsevier, 2007.

[28] B.-Z. Zhan *et al.*, "Control of particle size and surface properties of crystals of NaX zeolite," *Chem. Mater.*, vol. 14, no. 9, pp. 3636–3642, 2002.

[29] Y. Zhan, X. Li, Y. Zhang, L. Han, and Y. Chen, "Phase and morphology control of LTA/FAU zeolites by adding trace amounts of inorganic ions," *Ceram. Int.*, vol. 39, no. 5, pp. 5997–6003, 2013.

[30] E. M. FLANIGEN, H. KHATAMI, and H. A. SZYMANSKI, "Infrared Structural Studies of Zeolite Frameworks," no. 28, pp. 201–229, 1974.

[31] A. Guzman, I. Zuazo, A. Feller, R. Olindo, C. Sievers, and J. A. Lercher, "On the formation of the acid sites in lanthanum exchanged X zeolites used for isobutane/cis-2-butene alkylation," *Microporous mesoporous Mater.*, vol. 83, no. 1–3, pp. 309–318,

2005.

[32] Z. Le, L. I. Qiang, Q. I. N. Yucai, and Z. Xiaotong, “Investigation on the mechanism of adsorption and desorption behavior in cerium ions modified Y-type zeolite and improved hydrocarbons conversion,” *J. Rare Earths*, vol. 34, no. 12, pp. 1221–1227, 2016.

[33] X. Du, X. Gao, H. Zhang, X. Li, and P. Liu, “Effect of cation location on the hydrothermal stability of rare earth-exchanged Y zeolites,” *CATCOM*, vol. 35, pp. 17–22, 2013.

[34] E. F. T. Lee and L. V. C. Rees, “Calcination of cerium (Ill) exchanged Y zeolite,” no. Ill, 1986.

[35] Y. Shanqing, T. Huiping, D. Zhenyu, Z. Yuxia, and L. Jun, “Different Influences of Lanthanum and Cerium on Stability of Y Zeolite and Their DFT Calculations,” vol. 13, no. 1, pp. 16–23, 2011.

[36] M. Thommes *et al.*, “Physisorption of gases, with special reference to the evaluation of surface area and pore size distribution (IUPAC Technical Report),” *Pure Appl. Chem.*, vol. 87, no. 9–10, pp. 1051–1069, 2015.

[37] S. Komaty *et al.*, “A facile route toward the increase of oxygen content in nanosized zeolite by insertion of cerium and fluorinated compounds,” *Molecules*, vol. 23, no. 2, 2018.

[38] X. Liu, S. Liu, and Y. Liu, “A potential substitute for CeY zeolite used in fluid catalytic cracking process,” *Microporous Mesoporous Mater.*, vol. 226, pp. 162–168, 2016.

[39] S. C. Laha, P. Mukherjee, S. R. Sainkar, and R. Kumar, “Cerium containing mcm-41-type mesoporous materials and their acidic and redox catalytic properties,” *J. Catal.*, vol. 207, no. 2, pp. 213–223, 2002.

[40] M. Guo, J. Lu, Y. Wu, Y. Wang, and M. Luo, “UV and visible Raman studies of oxygen vacancies in rare-earth-doped ceria,” *Langmuir*, vol. 27, no. 7, pp. 3872–3877, 2011.

[41] Y. Peng *et al.*, “Investigation of the Poisoning Mechanism of Lead on the CeO2瑎WO3 Catalyst for the NH3–SCR Reaction via in Situ IR and Raman Spectroscopy Measurement,” *Environ. Sci. Technol.*, vol. 50, no. 17, pp. 9576–9582, 2016.

[42] C. R. Moreira, M. Schmal, and M. M. Pereira, “The effect of cerium introduction on vanadium-USY catalysts,” in *Studies in Surface Science and Catalysis*, vol. 143, Elsevier, 2000, pp. 915–923.

[43] J. Li *et al.*, “Tuning of acidity in CeY catalytic cracking catalysts by controlling the migration of Ce in the ion exchange step through valence changes,” *J. Catal.*, vol. 329, pp. 441–448, 2015.

[44] V. A. Online, “A DFT + U study of NO evolution at reduced CeO 2 (110) †,” vol. 2, no. 110, pp. 16904–16908, 2014.

[45] E. Ito *et al.*, “Selective reduction of NO , with ammonia over cerium-exchanged

mordenite," vol. 4, no. 94, pp. 95–104, 1994.

[46] A. Akah, "Application of rare earths in fluid catalytic cracking : A review," *J. Rare Earths*, vol. 35, no. 10, pp. 941–956, 2017.

[47] X. Du, X. Gao, H. Zhang, X. Li, and P. Liu, "Effect of cation location on the hydrothermal stability of rare earth-exchanged Y zeolites," *Catal. Commun.*, vol. 35, pp. 17–22, 2013.